IEEE Access
Multidisciplinary | Rapid Review | Open Access Journal

IEEE POWER & ENERGY SOCIETY SECTION

Received 18 October 2023, accepted 23 November 2023, date of publication 30 November 2023,
date of current version 15 December 2023.

Digital Object Identifier 10.1109/ACCESS.2023.3338361

RESEARCH ARTICLE

Enhanced Energy Delivery for Solar PV Distributed Generators at Voltage Sags

FAUZAN ISMAIL, JAFFERI JAMALUDIN, (Member, IEEE), AND NASRUDIN ABD RAHIM, (Senior Member, IEEE)

Higher Institution Centre of Excellence (HICoE), UM Power Energy Dedicated Advanced Centre (UMPEDAC), University of Malaya (UM), Kuala Lumpur 59990, Malaysia

Corresponding author: Nasrudin Abd Rahim (nasrudin@um.edu.my)

This work was supported in part by the University of Malaya Power Energy Dedicated Advanced Center (UMPEDAC) and the Higher Institution Center of Excellence (HICoE) Program Research under Grant UMPEDAC-2020 (MOHE HICOE-UMPEDAC), in part by the Ministry of Education Malaysia through the University of Malaya under Grant PPSI-2020-INDUSTRI-CREST01.

ABSTRACT Distributed generator of renewable energy (DGRE) requires ancillary services for protection against disturbances in the grid system. Hence, a current limiting property is crucial for the DGRE to achieve self-protection. However, such property would reduce the generated power that corresponds to optimum current injection. In order to overcome this shortcoming, this paper proposes an enhanced DGRE that features decoupled active and reactive power delivery as well as low voltage ride-through (LVRT) strategy. An improved DGRE power delivery system is achieved by employing an auto-correction droop control scheme. By taking into account the droop slope parameters, the system adjusts the reference voltage based on the power value computed from the measured voltage and current. Active and reactive power are consequently delivered proportionally, while the voltage at the point of common coupling (PCC) is maintained despite a voltage sag. In addition, the LVRT strategy which involves three modes namely Constant Average Active Power Control (CAAPC), Constant Active Current Control (CACC), and Constant Peak Current Control (CPCC) would ensure that the grid code requirements are met and the DGRE would remain connected to the grid during a voltage sag. By generating the necessary active and reactive power, the grid voltage can be satisfactorily restored. In the event of a grid fault, the combination of the proposed auto-correction droop control scheme and LVRT strategy would enhance power delivery and increase voltage stability. The DGRE prototype has been developed and experimental tests have been conducted for validation purposes. Both strategies have been practically implemented by the DGRE with satisfactory performance achieved.

INDEX TERMS Droop control, power delivery, LVRT, renewable energy sources, voltage sag.

I. INTRODUCTION

Increasing the number of distributed generators (DGs) connected to the primary grid will result in adverse effects if they are disconnected simultaneously under fault conditions. There may be a reduction in power dispatch and an increase in system instability as a result of this situation. It is important that the DGs remain connected during disturbances in order to maintain the continuity of the primary grid. Inverter units must be equipped with fault tolerance capabilities in order to meet this additional requirement [1]. Initially, a current limiter was applied to provide protection for the inverter in the event of a disturbance. A policy was then issued by IEEE on the application of low voltage ride-through (LVRT) within the inverter control algorithm. LVRT and reactive power injection have demonstrated their ability to maintain grid connection and to support voltage collapse in the grid [2].

In the past, the inverter used the LVRT strategy in order to increase reactive current injection (RCI) with reduced active power while simultaneously managing the safety of the power

The associate editor coordinating the review of this manuscript and approving it for publication was Emilio Barocio.

system. However, this strategy requires the transmission network to have an inductive impedance in order to achieve voltage stability. In addition, LVRT methods that employ active power curtailment control could limit power generation from the DGRE, which may cause frequency instability and local energy shortages. DGRE performance can be improved under voltage sag by maintaining DC currents with DC-Link voltage control [3]. The DC chopper and active current limiter control can also improve performance by maintaining P_{dc}, I_{dc}, and V_{dc} to regulate active (P) and reactive power (Q) injections during voltage sags [4].

The DGRE can maintain the grid voltage at the PCC by injecting P and Q. This situation relates to the injection of reactive current to cope with the disturbance in the grid. Consequently, the inverter should limit the generated current in accordance with the inverter's rated current in order to avoid potential instability. Current-limiting strategies and related controls can be applied using a synchronous reference frame (dq-frame), stationary reference frame ($\alpha\beta$-frame), or natural reference frame (ABC-frame) [5], [6]. By limiting the current magnitude, a current-limiting inverter can successfully ride through these disturbances, support the power grid, and recover power after the trouble has been resolved [7].

In grid-supporting inverters, the droop control scheme is commonly used to maintain unbalanced loads, restore grid voltage, and inject proportional amounts of P and Q [8], [9], [10], [11], [12], [13], [14]. Since the line impedance affects the distributed generator power-sharing accuracy and stability, the droop control scheme with virtual impedance, complex virtual impedance, adaptive virtual impedance, adaptive complex virtual impedance, and estimated virtual impedance were introduced to improve the power-sharing performance of the distributed generator [8], [12], [13]. Nevertheless, in [15], an adaptive droop control scheme was discussed, asserting that a suitable voltage reference could enhance the power-sharing accuracy with seamless transitions [16]. Utilizing the measured voltage coupling, it determines the reactive power requirement. Additionally, the adjustment of the droop slope coefficient also contributes to the improvement of power-sharing accuracy. For distributed generators, both dq-frame voltage reference adjustments provide proportional sharing of P and Q.

In the light of this development, the droop control strategy appears to be reliable if it is incorporated into the distributed generator system. However, a protection scheme is necessary in order to limit the amount of power that can be delivered. In this paper, the proposed protection scheme incorporates the LVRT algorithms and the droop control strategy in order to satisfy the grid code requirements to be discussed later in the paper. Based on DGRE's capability to deliver the active and reactive power proportionally, the auto-correction droop control scheme is assigned to restore voltage after a sag [17] In addition to addressing the voltage drop, the DGRE may also utilize the LVRT algorithm in order to maintain grid connectivity. The key contributions of this paper can be summarized as follows:

1. The proposed strategy enhances power delivery under various grid voltage sag conditions by employing a suitable operation selected from among the auto-correction droop control scheme and three LVRT modes based on DGRE apparent power, required reactive current injection and criticality of the voltage sag.
2. The proposed droop control scheme is equipped with auto-correction feature that provides voltage restoration capability and overcurrent protection to satisfactorily restore the voltage at the PCC under grid voltage drops.
3. The proposed auto-correction droop control features a seamless and fast response in restoring the grid voltage effectively after the occurrence of voltage sags and introduces adaptive power control to proportionally regulate active and reactive power in accordance with network impedance.
4. The proposed LVRT strategy ensures continuing grid connectivity in the event of a voltage drop on the grid via a combination of three modes namely Constant Average Active Power Control (CAAPC), Constant Active Current Control (CACC), and Constant Peak Current Control (CPCC) that maximizes power delivery with overcurrent protection.

The following structure is followed in this paper. Section II describes the proposed system model, control methods, and strategies. Section III details the specific strategies that are selected to enhance power delivery under voltage sag conditions. In Section IV, experimental results are presented as well as discussions of the results are provided As a final note, Section V concludes with concluding remarks.

II. SYSTEM DESCRIPTION AND CONTROL STRATEGY

Figure 1 depicts the DGRE power circuit, which supports the local load both under normal and grid fault conditions. It consists of an inverter, a filter unit, and a local load connected to the grid via a transformer. The inverter consists of three control loops namely power, voltage, and current loops. The modulated voltage generated by the inverter is denoted by V_i, which refers to the unfiltered inverter voltage, contributing to harmonics. The inverter is connected to the LC filter, composed of capacitor C_f and inductance L_f with parasitic resistance R_l and R_c. To achieve synchronization, a filtered inverter voltage with reduced harmonics as represented by $E\angle\delta$ should be aligned with the grid voltage $V_g\angle 0°$ with zero phase angle. Once synchronization has been achieved, S_1 is switched on to activate the grid-connected mode, which then connects the inverter to the primary grid with power angle δ. Meanwhile, the impedance Z connected in series to the networks represents the resistance and reactance of the networks.

Generally, inverter algorithms use droop control, whether they are operating normally or in fault conditions. By injecting reactive power into the grid, droop control can

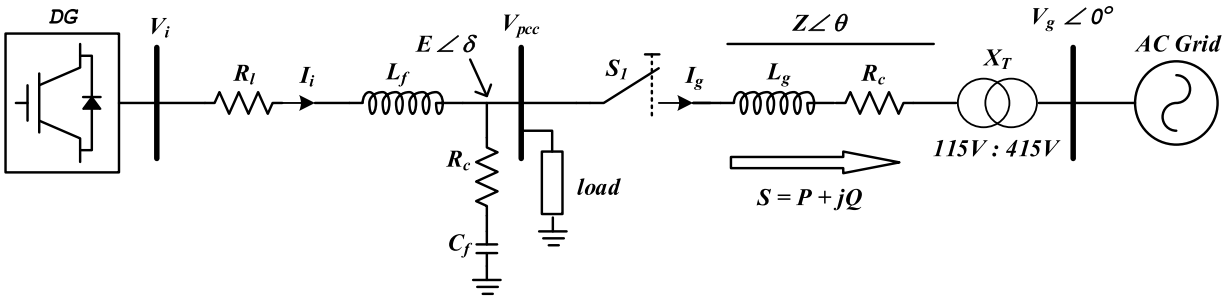

FIGURE 1. A power circuit of the system.

compensate for voltage drops and restore grid voltages to their normal magnitude. As a result, operations are limited to the inverter's power source, and the inverter will be disconnected when its limits are exceeded. Thus, the LVRT strategy can be adopted to maintain power delivery from the inverter to the grid while remaining connected. Figure 2 illustrates the flow chart of the inverter action during the grid voltage drops.

Initally, the DGRE sets the parameters and measures the inverter voltage, inverter current, and grid voltage which are denoted as $V_{i_{abc}}$, $I_{i_{abc}}$, and $V_{g_{abc}}$, respectively. These are used to determine P, Q, S, and $V_{g\ pu}$ in which the rated grid voltage (115 V) is equivalent to 1.0 pu. Based on the grid code, the voltage can be divided into four levels. V_g more than 1.1 pu is categorized as over voltage, $0.9 < V_g < 1.1$ is known as the normal voltage range, voltage sag is when $0.5 < V_g < 0.9$, and critical voltage sag happens when $V_g < 0.5$. An auto-correction droop control algorithm is employed to ensure a proportional injection of P and Q under normal grid voltage conditions. During voltage sag, the inverter evaluates the apparent power (S), and determines whether it should operate as a voltage restorer utilizing an auto-correction droop control scheme or as an LVRT. For LVRT strategy, Constant Average Active Power Control (CAAPC), Constant Active Current Control (CACC), and Constant Peak Current Control (CPCC) can be selected in accordance with the inverter's maximum generated power.

Referring to the power model for the distributed generator of the grid-connected inverter as shown in Figure 1, P and Q are defined as in (1) – (4) respectively,

$$P = \left(\frac{EV_g}{Z}\cos\delta - \frac{V_g^2}{Z}\right)\cos\theta + \frac{EV_g}{Z}\sin\delta\sin\theta \quad (1)$$

$$Q = \left(\frac{EV_g}{Z}\cos\delta - \frac{V_g^2}{Z}\right)\sin\theta - \frac{EV_g}{Z}\sin\delta\cos\theta \quad (2)$$

Given a very small or almost zero value for δ, which implies that cos δ is approximately equal to 1 and sin δ is approximately equal to δ, thus

$$P = \left(\frac{EV_g}{Z} - \frac{V_g^2}{Z}\right)\cos\theta + \frac{EV_g}{Z}\delta\sin\theta \quad (3)$$

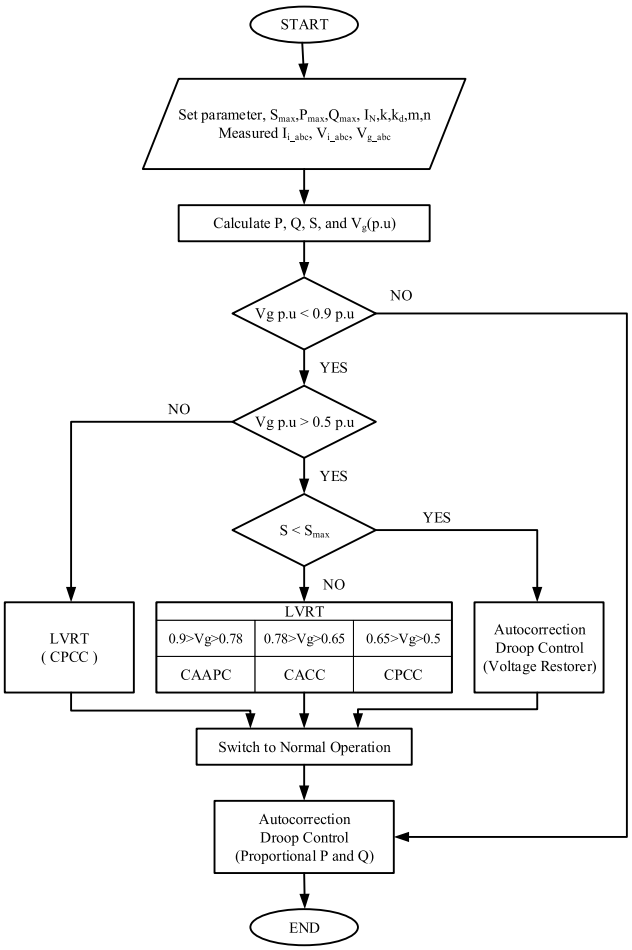

FIGURE 2. Flow diagram of the proposed strategy.

$$Q = \left(\frac{EV_g}{Z} - \frac{V_g^2}{Z}\right)\sin\theta - \frac{EV_g}{Z}\delta\cos\theta \quad (4)$$

The impedance angle θ influences the variation of the decoupling input and output. Due to θ equals $\pi/2$ rad and the impedance being inductive, P and δ are therefore approximately proportional. It is important to highlight that in this scenario, Q and E are also roughly proportional. In order to achieve droop control, reducing frequency relates

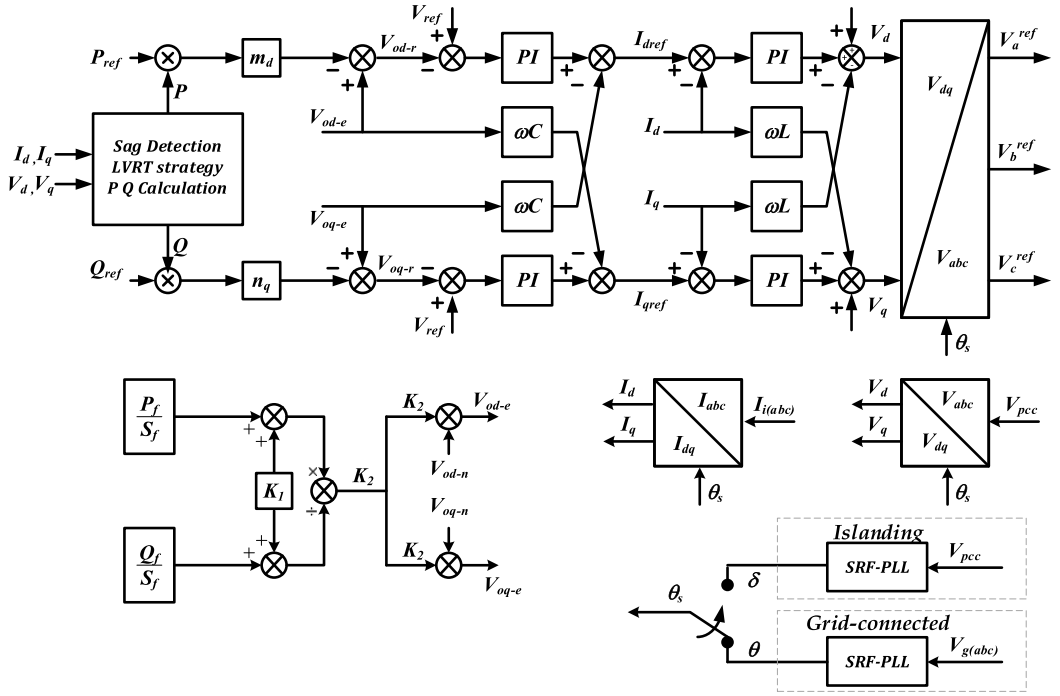

FIGURE 3. Block diagram of the proposed system.

to increasing active power and reducing voltage involves increasing reactive power [18].

With reference to Figure 3, the filtered values of P and Q can be obtained by utilizing equations (5) and (6) respectively. The instantaneous active power (P_o) defined in equation (7) and the instantaneous reactive power (Q_o) defined in equation (8) are computed based on the measured output current I_{odq} and output voltage V_{odq} as described below [19]:

$$P_f = \frac{\omega_c}{s+\omega_c} P_o \tag{5}$$

$$Q_f = \frac{\omega_c}{s+\omega_c} Q_o \tag{6}$$

$$P_o = 1.5\left(V_{od} I_{od} + V_{oq} I_{oq}\right) \tag{7}$$

$$Q_o = 1.5\left(V_{oq} I_{od} - V_{od} I_{oq}\right) \tag{8}$$

where, ω_c, P_f and Q_f are the cut-off frequency of low-pass filter,the filtered instantaneous P and Q, respectively.

It is possible to use active-reactive power (PQ) control to support the grid, which involves maintaining a specific relationship between the injected current and the voltage at the interconnection point. Depending on the current state of the grid, active or reactive power can be delivered. As a result of abnormal network conditions, voltage amplitude and phase angle fluctuations may occur at the point of interconnection of the inverter. In the event of an undervoltage condition, the inverter adjusts its output voltage by injecting a corresponding amount of reactive power into the network [20].

According to E.ON grid code [21], the maximum amount of active power that can be produced by the three-phase inverter, denoted as P_{i_max}, is subject to certain limits during a grid sag period and can be calculated as follows [22]:

$$P_{i\_max} = S_{i\_max} \times \cos\left(tan^{-1}\frac{I_{q_{ref}}}{\sqrt{I_{rated}^2 - I_{q_{ref}}^2}}\right) \tag{9}$$

The rated apparent power of the three-phase inverter is represented by $S_{i\_max} = 3V_{i_{rated}} \cdot I_{i\_max}$, while the required reactive current is denoted as $I_{q_{ref}}$, and I_{rated} represents the inverter rated current.

It is common for PV inverters to have spare capacity for compensating reactive power since they often operate at lower power levels than their rated power. To determine the maximum reactive power available Q_{i_max} can be calculated as follows [23]:

$$\left|Q_{i\_max}\right| = \sqrt{S_{i\_max}^2 - P_{i\_max}^2} \tag{10}$$

A. THE PROPOSED DROOP CONTROL STRATEGY

The proposed approach introduces an auto-correction term for the nominal voltage, referred to as V_{od-e} and V_{oq-e}, which aims to enhance the P-Q-V droop control in the following manner:

$$\begin{cases} V_{od-r} = V_{od-e} - m_p P_f \\ V_{oq-r} = V_{oq-e} - n_q Q_f \end{cases} \tag{11}$$

where, coefficient of the droop slope for P and Q are denoted as m_p and n_q, respectively.

The respective DG independently calculates V_{od-e} and V_{oq-e} by measuring the necessary local parameters. The

equations used to compute V_{od-e} and V_{oq-e} are as follows:

$$\begin{cases} V_{od-e} = K_2 V_{od-n} \\ V_{oq-e} = K_2 V_{oq-n} \end{cases} \tag{12}$$

The inverter can automatically detect changes in load within the network. This function is useful to determine the inverter's output power against the load changes anywhere in the network. Therefore, this algorithm is utilized for synchronizing changes to P and Q.

The calculated instantaneous active and reactive power in equations (5) to (8) are utilized to determine the apparent power $S_f = \sqrt{P_f^2 + Q_f^2}$, which is used to calculate K_2 as a unitless parameter.

$$K_2 = \frac{K_1 + \left(\frac{P_f}{S_f}\right)}{K_1 + \left(\frac{Q_f}{S_f}\right)} \tag{13}$$

K_1 is a constant, and per unit of P_f and Q_f are represented by $P_{(pu)}$ and $Q_{(pu)}$ which are expressed as below:

$$P_{(pu)} = \frac{P_f}{S_f} \tag{14}$$

$$Q_{(pu)} = \frac{Q_f}{S_f} \tag{15}$$

(14) and (15) are used in (13) to calculate K_2 and are substituted into the equations in (11) and (12). As illustrated in Figure 3, equations (16) and (17) provide the voltage references.

$$V_{od-r} = \frac{K_1 + P_{(pu)}}{K_1 + Q_{(pu)}} V_{od-n} - m_p P_f \tag{16}$$

$$V_{oq-r} = \frac{K_1 + P_{(pu)}}{K_1 + Q_{(pu)}} V_{oq-n} - n_q Q_f \tag{17}$$

Since V_{ref} is identified as the inverter reference voltage, hence, the voltage error can be written as:

$$\dot{V}_{xd} = V_{ref} - \left(K_2 V_{od} - m_d P_f\right) \tag{18}$$

$$\dot{V}_{xq} = V_{ref} - \left(K_2 V_{oq} - n_q Q_f\right) \tag{19}$$

In the steady state, $\dot{V}_{xd}$ and $\dot{V}_{xq}$ are very small and almost zero. Consequently:

$$\begin{aligned} m_d P_f &= K_2 V_{od} - V_{ref} \\ n_q Q_f &= K_2 V_{oq} - V_{ref} \end{aligned} \tag{20}$$

In other words, the actual voltage for V_{od} and V_{oq} are given below:

$$V_{od} = \frac{m_d P_f - V_{ref}}{K_2} = V_{ref} \frac{m_d P_f}{K_2 V_{ref}} - \frac{V_{ref}}{K_2} \tag{21}$$

$$V_{oq} = \frac{n_d Q_f - V_{ref}}{K_2} = V_{ref} \frac{n_d Q_f}{K_2 V_{ref}} - \frac{V_{ref}}{K_2} \tag{22}$$

Thus, $\frac{m_d P_f}{V_{ref}}$ and $\frac{n_q Q_f}{V_{ref}}$ represent the ratios of voltage drop for active and reactive components, respectively.

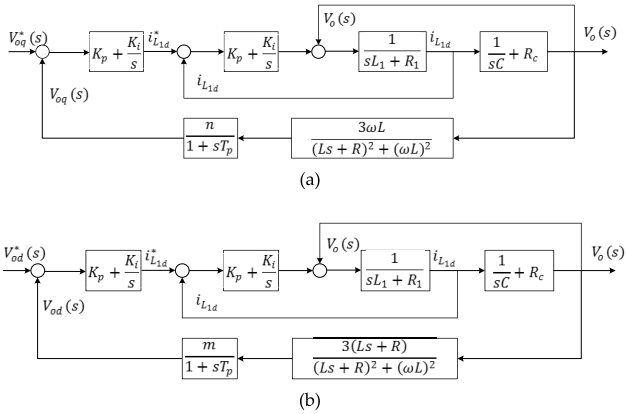

FIGURE 4. The control diagram of the overall system, (a) d-frame, (b) q-frame.

B. SMALL SIGNAL MODEL OF THE PROPOSED SYSTEM

The dynamic stability of droop controllers is greater than that of voltage and current control loops. The reference voltage used to control the output voltage of the inverter is generated by a droop control technique. Thus, referring back to Figure 1, equations (1) – (4) can be expressed as the following:

$$P = \frac{3}{R^2 + X^2}\left(RE^2 - REV_g \cos\delta + XEV_g \sin\delta\right) \tag{23}$$

$$Q = \frac{3}{R^2 + X^2}\left(XE^2 - XEV_g \cos\delta - REV_g \sin\delta\right) \tag{24}$$

The resistive component is represented by R, while the inductive component is represented by X. Then assuming a small power angle, hence $\sin\delta \approx 0$ and $cos\delta \approx 1$. Therefore, the equations can be simplified as follows:

$$P = \frac{3}{R^2 + X^2}\left(RE^2 - REV_g\right) \tag{25}$$

$$Q = \frac{3}{R^2 + X^2}\left(XE^2 - XEV_g\right) \tag{26}$$

According to the small-signal models presented in [24] and [25], a straightforward way to calculate the active power of the inverter output is as follows:

$$P = \frac{3\,(Ls + R)}{(Ls + R)^2 + (\omega L)^2}\left(E^2 - EV_g\right) \tag{27}$$

$$Q = \frac{3\omega L}{(Ls + R)^2 + (\omega L)^2}\left(E^2 - EV_g\right) \tag{28}$$

Considering small perturbations around the state-steady point, the linear equations are as follows:

$$\Delta P = \frac{3\,(Ls+R)\,E}{(Ls+R)^2+(\omega L)^2}\Delta E + \frac{3\omega L E^2}{(Ls+R)^2+(\omega L)^2}\Delta\delta \tag{29}$$

$$\Delta Q = \frac{3\omega L E}{(Ls+R)^2+(\omega L)^2}\Delta E + \frac{-3\,(Ls+R)\,E^2}{(Ls+R)^2+(\omega L)^2}\Delta\delta \tag{30}$$

As shown in Figure 4, the proposed control system is configured according to equations (29) and (30), as well as Figure 3. Based on feedback power and auto-correction gain

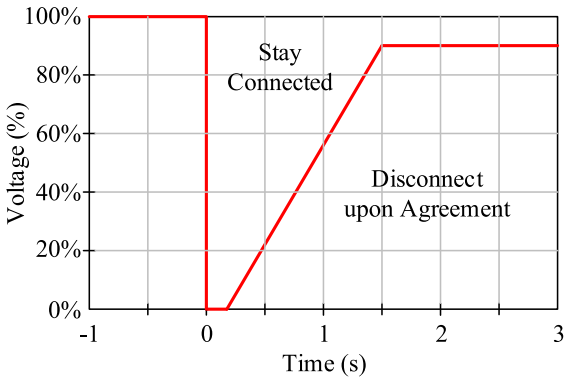

(a)

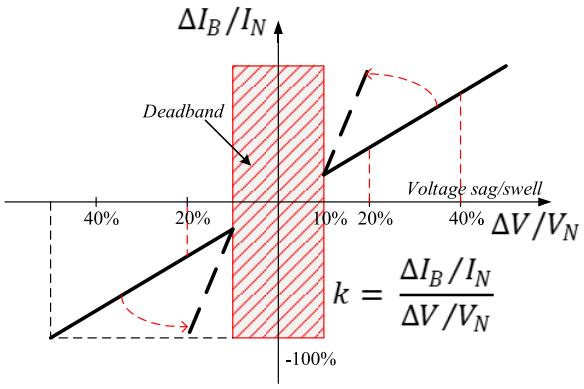

(b)

FIGURE 5. Requirement for a German grid code (a) LVRT Curve (VDE-AR-N 4120), (b) Region for reactive power injection.

K_2 in (11), the proposed system generates voltage reference. Consequently, the simplified transfer function of $H_d(s) = \left(\frac{V_{od}}{V_{od}^*}\right)$ and $H_q(s) = \left(\frac{V_{oq}}{V_{oq}^*}\right)$ can be written as (31) and (32), shown at the bottom of the page.

Finally, Figure 4 shows the block diagram of the overall system, which consists of a voltage loop, a current loop, and an outer power loop.

C. GRID CODE REQUIREMENT

In accordance with the previous grid code requirement, distributed generators (DGs) must disengage from the grid when the grid voltage drops occur and reconnect to the grid following the resolution of the fault [26], [27]. Microgrids, however, are required to provide active power along with reactive power injection capabilities during grid voltage drops in order to minimize the risk of instability [28].

According to Figure 5(a), a severe grid drop voltage below the red curve may result in DG being disconnected from the primary grid. By injecting a specific quantity of reactive power above the curve, the system can remain connected. A 1% drop in grid voltage below $0.9V_N$ necessitates a leastwise k% additional current injection, as shown in Figure 5(b). The system should be able to supply 1 pu. of reactive current if required. The following are the related equations:

$$I_{q_{ref}} = \begin{cases} 0, & 0.9\ V_N < V_g \\ k\left(1 - \dfrac{V_g}{V_N}\right) I_N, & 0.5\ V_N \le V_g < 0.9\ V_N \\ I_N, & V_g \le 0.5\ V_N \end{cases} \tag{33}$$

where V_N denotes nominal grid voltage, I_N denotes the rated current of the converter, ΔV denotes the extent of grid voltage drops, ΔI_B denotes the increase in reactive current following a defect, and k is a constant that should be greater or equal to 2 p.u.

A voltage detection method based on the Conventionally Synchronously Rotating Reference Frame (CSRRF) [29] is illustrated in Figure 6. This method detects voltage sag by utilizing the $abc - dq$ transformation to calculate DC quantities (V_d, V_q) proportional to AC quantities of the grid voltages (V_a, V_b, V_c) which can be expressed as:

$$\begin{bmatrix} V_d \\ V_q \end{bmatrix} = \frac{2}{3} \begin{bmatrix} \cos\omega t & -\sin\omega t \\ \sin\omega t & \cos\omega t \end{bmatrix} \begin{bmatrix} 1 & -1/2 & -1/2 \\ 0 & \sqrt{3}/2 & -\sqrt{3}/2 \end{bmatrix} \begin{bmatrix} V_a \\ V_b \\ V_c \end{bmatrix} \tag{34}$$

As shown in Figure 6, the sag signal is generated from a filtered $V_{dq} = \sqrt{V_d^2 + V_q^2}$ which is then compared with a DC reference in the comparator (i.e., 0.9 pu.). Here, V_{dq} varies according to measured grid voltage, and a Low Pass Filter (LPF) is utilized to eliminate 100 Hz component or 2ω.

In reference [30], the absolute difference (k_{sag}^t) between the load voltage and the actual terminal voltage is calculated.

$$k_{sag}^t = \left|1 - \sqrt{V_d^2 + V_q^2}\right| \tag{35}$$

D. COMPARISON OF TECHNIQUES TO HANDLE GRID VOLTAGE DROPS

Table 1 summarizes the previous research proposed by various authors. The inverter can provide ancillary services, such as handling grid voltage sag, by injecting appropriate reactive power. However, inverters require a higher current to support grid voltage, especially in critical sag conditions.

$$H_d(s) = \frac{3mLs + 3mR}{T_pLs^3 + \left(2L + 2T_pLR\right)s^2 + \left(2LR + T_pR^2 + T_p\omega^2L^2\right)s^2 + R^2 + \omega^2L^2} \tag{31}$$

$$H_q(s) = \frac{3n\omega L}{T_pLs^3 + \left(2L + 2T_pLR\right)s^2 + \left(2LR + T_pR^2 + T_p\omega^2L^2\right)s^2 + R^2 + \omega^2L^2} \tag{32}$$

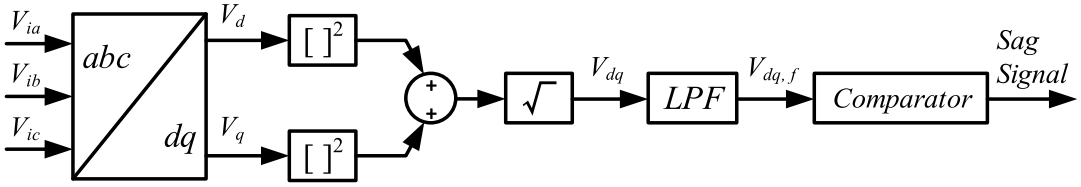

FIGURE 6. CSRRF-based voltage sag detection.

TABLE 1. Comparison of techniques to handle voltage sag.

Author	Method	Over current protection	Voltage Sag		Validation	Note
			Voltage Restorer	LVRT mode		
[31]	LVRT, PCL, APRC	✓	×	✓	Experiment	Smooth during transition and fast recovery
[30]	DVR	×	✓	×	Experiment	Spikes during transition and fast recovery
[28]	LVRT, CDC-VI	×	✓	✓	Experiment (dSPACE)	Fast dynamic response
[3]	LVRT, MPPT, ACI, Adaptive DC-Link voltage	×	×	✓	Experiment (TMS320F28035)	Spike during transition, Enhance P injection with extra energy store in DC capacitor
[32]	LVRT, CAAPC, CACC, CPCC	✓	×	✓	Experiment	Smooth during transition
[33]	APC, RPI	✓	×	✓	Experiment (TMS320F28335)	Delay 0.02s during transition,
[34]	FRT	✓	✓	✓	Simulation	Smooth transition and recovery, without delay
[35]	LVRT, MOCS	✓	✓	✓	Simulation	Smooth during transition and fast recovery
[36]	LVRT, CALC	✓	×	✓	Experiment	Smooth during transition and fast recovery
[37]	LVRT, CAAPC, CACC, CPCC	✓	×	✓	Simulation	Smooth during transition and fast recovery
[38]	LVRT, MPPT, AAPC, CACC, CPCC	✓	×	✓	Experiment	Smooth during transition
[39]	FRT, CLD	✓	×	✓	Experiment	More than ten cycles restore to a stable current after LVRT.
[40]	DVR	×	✓	×	Experiment	Smooth during transition and fast recovery
This paper	LVRT, ADC	✓	✓	✓	Experiment	Smooth during transition and fast recovery

Note:
PCL = Peak Current Limit
APRC = Active Power Ripple Cancelation
DVR = Dynamic Voltage Restorer
CDC-VI = Conventional Droop Control and Virtual impedance
MPPT = Maximum Power Point Tracking
ACI = Active Current Injection
CAAPC = Constant Average Active Power Control
CACC = Constant Active Current Control
CPCC = Constant Peak Current Control
APC = Active Power Curtailment
RPI = Reactive Power Injection
MOCS = Multi-Objective Control Strategy
CALC = Current Amplitude Limitation Control
CLD = Current Limiting Droop
LVRT = Low Voltage Ride Through
ADC = Auto-correction Droop Control

A multifunctional inverter must therefore be protected by LVRT and current limiting strategies.

LVRT strategy ensures the interconnection of inverters to the primary grid. It sustains power delivery during voltage sag, in which the constant average active power control [32], [37], [38] and the adaptive DC link-voltage with MPPT algorithm [3] regulate the maximum active power injection. Overshoot currents, however, appear on the falling edge of voltage sags. Thus, the inverter must provide overcurrent protection, such as constant peak current control [31], [32], [36], [37], [38], active power curtailment [33] and constant active current control [32], [37], [38]. Another approach to droop control is the LVRT mode with features such as limiting current strategy [39] and voltage restorer [28]. Dynamic voltage restorer (DVR) in particular has a function to support the grid voltage drop by restoring the nominal voltage [30], [40].

A simulation of an inverter with LVRT and voltage restorer capability during grid voltage sag is presented by [34] and [35]. Additionally, the methods considered current limits for overcurrent protection during voltage sags. A similar objective has been achieved with the proposed auto-correction droop control, which provides voltage restoration capability and overcurrent protection. Inverters limit the amount of reactive current injected during voltage sags in order to restore the voltage at the PCC.

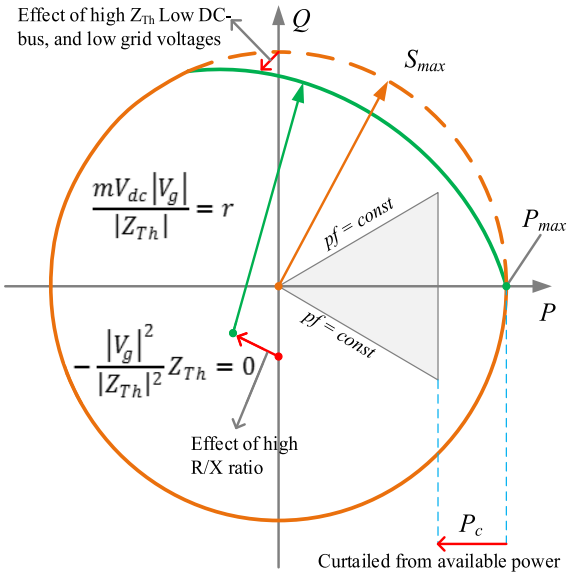

FIGURE 7. Operating region of DGRE with high Z_{Th} and R/X ratio [41].

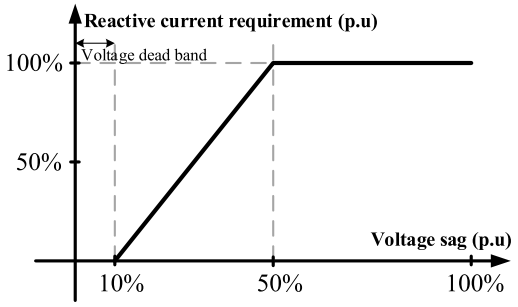

FIGURE 8. The required reactive current injection of E.ON grid connection requirement (Germany) [21].

III. ENHANCED POWER DELIVERY UNDER VOLTAGE SAG

The traditional protection scenario of the grid-connected inverter under grid fault conditions uses an anti-islanding strategy to ensure that the inverter is disconnected from the grid. As part of the grid code requirement IEEE 1547, the LVRT feature is introduced to allow the inverter to remain connected in the event of a voltage drop on the grid. In addition, the distributed generator droop control is also introduced in order to regulate P and Q under unbalanced grids and voltage drops on the grid. Droop control can restore the voltage drop, but it limits the amount of power generated. LVRT is used in conjunction with droop control strategy to maximize power delivery into the grid. When voltage sag occurs, LVRT and droop control work in accordance with power and current levels, respectively.

A. VOLTAGE RESTORER CAPABILITY

Adaptive power control is used to regulate P and Q based on network impedance when autocorrection droop control is used. In this method, a maximum power is used to generate reactive power in order to restore the PCC voltage during sag disturbances. If it is unable to inject enough reactive power as a result of power source limitations, the droop control strategy may result in another system failure. As shown in Figure 7, the DGRE maximum energy capacity must be reduced to provide sufficient margin [41].

According to Figure 7, the DGRE attempts to reduce active power associated with peak current curtailments when providing reactive power to the primary grid [42], [43]. DGRE power losses can have more severe consequences than grid voltage drops due to the increasing penetration of DGRE power. In accordance with IEEE Std. 1547-2018 [43], during a grid voltage drop, the inverter should provide reactive power and remain connected to the grid. For persistent voltage drops, the inverter must be disconnected.

Peak current curtailments to prevent exceeding active power injection are represented by a circle with a S_{max} radius in Figure 7. Thus, the DGRE provides power to the primary grid as follows:

$$S = P + jQ = \frac{k_m V_{dc} |V_g| e^{-j\delta} - |V_g|^2}{Z_{Th}^*} \tag{36}$$

where line-to-line RMS voltage of the inverter, line-to-line RMS voltage of the grid, phase angle between inverter and grid, and the complex conjugate of the Thevenin equivalent impedance of the grid are $k_m V_{dc}$, V_g, θ, and $Z_{Th}^* = |Z_{Th}| e^{-j\theta z}$, respectively. Meanwhile, variables such as the voltage at the dc-bus (V_{dc}) and the modulation index (m), as well as the network impedance, determine the amount of P and Q available to the inverter at any given time [44], [45], [46].

A distributed generation converter (DG converter) is typically required by the grid code to supply the necessary reactive current in order to maintain grid voltage in the event of a decrease in voltage. According to Figure 8, E.ON specifies the reactive current based on the remaining voltage (V) and rated current (I_{rated}) of the DG converter [21].

B. LVRT CAPABILITY

Traditionally, the IEEE 1547 standard assigns the DERs regulations that provide active power control for interconnection to electric power systems [23]. In spite of this, enhanced standards allow injecting reactive power in a range that is acceptable for maintaining voltage levels. Under normal grid conditions, the DGRE must be capable of supplying active power to the grid and injecting reactive power with overcurrent protection. The level of grid voltage determines the amount of reactive current injections.

$$\begin{cases} I_q = I_N, & 0 \le v_g < \left(1 - \frac{1}{k}\right) pu. \\ I_q = k\left(1 - v_g\right) I_N, & \left(1 - \frac{1}{k}\right) pu. \le v_g < 0.9\ pu. \end{cases} \tag{37}$$

According to the German grid code in Figure 5(a), the DGRE should be capable of detecting grid voltage drops

and injecting reactive power to the primary grid through the Reactive Power Injection (RPI) scheme [47]. As part of fault ride-through operations, the DGRE assigns injected reactive current in accordance with the grid voltage range [47]. The initial reactive current under a normal grid and the per unit (pu.) of instantaneous voltage under voltage sag are denoted as I_{q0} and v_g, respectively. Therefore the relationship can be written as:

$$k = \frac{\frac{(I_q - I_{q0})}{I_N}}{(1 - v_g)}, \text{ when } I_q < I_N \tag{38}$$

where $k \geq 2\ p.u.$

$$I_{g\ max} = \sqrt{I_d^2 + I_q^2} \leq I_{max} \tag{39}$$

The proposed RPI strategies are based on equations (37) and (39), where the current is in active mode. The peak magnitude of injected current, and the peak level of allowable current for the inverter are denoted as I_d, $I_{g\ max}$, I_{max}, respectively.

1) CONSTANT AVERAGE ACTIVE POWER CONTROL (CAAPC)

In the LVRT mode, the RPI scheme is designed to enhance power delivery to support the primary grid. The objective of this scheme is to maintain the average active power at a steady level over a short period of time. It can be expressed as

$$P = \frac{3}{2} V_{gm} I_d \tag{40}$$

where the amplitude of grid voltage and injected active current are represented by v_{gm} and I_d, respectively. In regular operations, the active current (I_d) is equivalent to the nominal current (I_N). Therefore, the average active power operated under LVRT mode with CAAPC scheme can be computed as $P = k_d P_N = (k_d/2)\, v_{gmn} I_N$. The nominal value of grid voltage is v_{gmn}, the nominal value of the current is I_N, and the output power reduction factor is k_d.

When the instantaneous grid voltage drops are within the range of $v_g : (1 - (1/k))\, pu. \leq v_g < 0.9\ pu.$, I_d and I_q can be defined as follows:

$$\begin{cases} I_d = \dfrac{k_d}{v_g} I_N \\ I_q = k\,(1 - v_g)\, I_N \end{cases} \tag{41}$$

where k is previously defined in Equation (38), the DGRE may continue to operate with CAAPC mode, although the grid voltage drops below $(1 - (1/k))$ pu. Based on the limits of the inverter current, the DGRE should entirely inject reactive power without active power (i.e., $I_q = I_N$). The dq frame of the inverter current can be defined as:

$$\begin{cases} I_d = \dfrac{k_d}{v_g} I_N \\ I_q = I_N \end{cases} \tag{42}$$

Nonetheless, the DGRE should consider overcurrent and overheating risks in order to maintain a constant output power, as shown in Equation (39). Under LVRT mode, the inverter must adhere to the constraints specified in equations (41) and (42).

$$\frac{1}{v_g} \sqrt{k_d^2 + k^2 \left(v_g - v_g^2\right)^2} \leq \frac{I_{max}}{I_N} \tag{43}$$

When $(1 - (1/k))\, pu. \leq v_g < 0.9\ pu.$, and

$$\frac{1}{v_g} \sqrt{k_d^2 + v_g^2} \leq \frac{I_{max}}{I_N} \tag{44}$$

when $v_g < (1 - (1/k))\ pu.$

2) CONSTANT ACTIVE CURRENT CONTROL (CACC)

As another option, the DGRE can maintain a constant active current of the RPI approach under LVRT operation. Referring to Equation (38), active current can be written as:

$$I_d = \frac{2P}{v_{gm}} = m I_N = const. \tag{45}$$

where m is a scaling factor ranging from $0 \leq m \leq 1\ pu.$ considering the design in case of derating operations. Referring to Equation (45), the RPI control approach responds to the voltage sag by reducing active power automatically, i.e., $P \propto v_{gm}$. Meanwhile, Equation (37) specifies the reactive current I_q. Therefore, I_d and I_q can be expressed as

$$\begin{cases} I_d = m I_N \\ I_q = k\,(1 - v_g)\, I_N \end{cases} \tag{46}$$

Here, the voltage range is defined as $(1 - (1/k))\ pu. \leq v_g < 0.9\ pu.$, where k is defined earlier. It is worth mentioning that the DGRE must inject full reactive power due to severe grid voltage drop. In such a scenario, I_d and I_q can be calculated as

$$\begin{cases} I_d = m I_N \\ I_q = I_N \end{cases} \tag{47}$$

where $v_g < (1 - (1/k))\ pu.$

The DGRE with CACC approach is possible to inject the surpass current as per Equation (39), which triggers the inverter to be tripped. In order to prevent this, the following requirements must be met:

$$\sqrt{m^2 + k^2 (1 - v_g)^2} \leq \frac{I_{max}}{I_N} \tag{48}$$

when $(1 - (1/k))\, pu. \leq v_g < 0.9\ pu.$, and

$$\sqrt{m^2 + 1} \leq \frac{I_{max}}{I_N} \tag{49}$$

when $v_g < (1 - (1/k))\ pu.$ For simplicity, the active current level can be regulated to match the rated current. (i.e., $m = 1$ pu., and $I_d = I_N$).

TABLE 2. Parameters of the proposed system.

Parameter	Value
Rated voltage of the DG (V)	115
Filter inductance L_c (mH)	5
Filter capacitance (uF)	10
Switching frequency f_{sw} (kHz)	20
Rate frequency f (Hz)	50
Droop coefficient m_p (red/s/W)	0.5
Droop coefficient n_q (V/Var)	0.05
Transformer ratio	115 : 415

3) CONSTANT PEAK CURRENT CONTROL (CPCC)

A PV inverter operating in LVRT mode can be at risk of overcurrent overloading due to the aforementioned RPI strategies. A CPCC control strategy has been proposed as a solution to this problem. During LVRT, the grid current peak is maintained continuously below the inverter current limit to prevent unintentional inverter shutdowns caused by overcurrent protection. In other words, the peak magnitude of injected current ($I_{g\ max}$) is equal to a constant value, which is equal to n times the nominal current (I_N), where n represents the peak current scaling factor. According to Equation (37), when the grid voltage is between the range of $\left(1-\left(1/k\right)\right)pu. \leq v_g < 0.9\ pu.$, the current in the dq-frame can be determined as below.

$$\begin{cases} I_d = \sqrt{n^2 - k^2\left(1-v_g\right)^2} I_N \\ I_q = k\left(1-v_g\right) I_N \end{cases} \tag{50}$$

If the grid voltage drops below $\left(1-\left(\frac{1}{k}\right)\right)\ pu.$, as stated in Equation (39), the current in the dq-frame must be:

$$\begin{cases} I_d = \sqrt{n^2 - 1} I_N \\ I_q = I_N \end{cases} \tag{51}$$

where v_g and k are defined previously.

It is essential to recognize that the value of n cannot exceed $I_{max}/I_N\ pu.$, which considers the inverter current protection as detailed in Equation (39). For instance, if an inverter is designed with a safety margin of 2 pu. (meaning $I_{max} = 2I_N$), the maximum value of n should be 2 pu. to maintain a stable RPI without triggering the inverter during LVRT operation. Therefore, if n is less than or equal to $\left(I_{max}/I_N\right)$, the PV inverter operation will not cause an increase in the amplitude of the injected grid current. At the same time, as stated in equations (40) and (50), the DGRE should provide adequate reactive power by reducing active power when operated in LVRT mode.

IV. RESULT AND DISCUSSION

The proposed strategy is tested experimentally in order to evaluate its effectiveness in enhancing power delivery in the event of grid voltage sag. As shown in Figure 9, an experimental prototype has been constructed. The values of the parameters used in the experiment are shown in Table 2. The test considers two scenarios. First, with the proposed

FIGURE 9. Prototype of the proposed system.

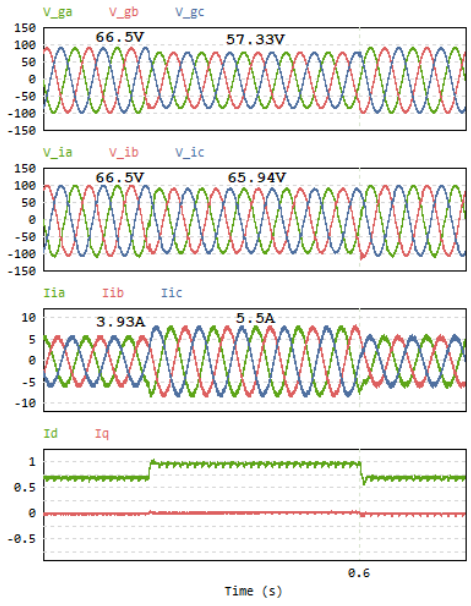

FIGURE 10. Simulation result of auto-correction droop control with V_g droop to 56.6V.

auto-correction droop control strategy based on the inverter capacity, the system should be able to support the PCC voltage. Second, the system should be able to operate using the LVRT strategy with curtailed power and overcurrent protection. In this case, the system is operated in accordance with the diagram shown in Figure 2.

Four ranges of the voltage sag level has been considered. For the first scenario, auto-correction droop control operates during the normal grid condition in which the grid voltage is within $0.9 > v_g > 0.78$. For the remaining voltage ranges, the second scenario which involves LVRT strategy applies: CAAPC mode for $0.9 > v_g > 0.78$, CACC mode for $0.78 > v_g > 0.65$, and CPCC mode for $0.65 > v_g > 0.5$. Combination of the two strategies provides an effective way to support the grid despite voltage sags.

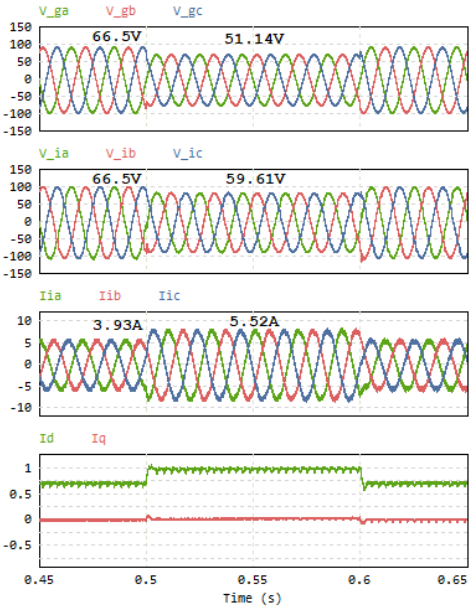

FIGURE 11. Simulation result of auto-correction droop control with V_g droop to 51.7V.

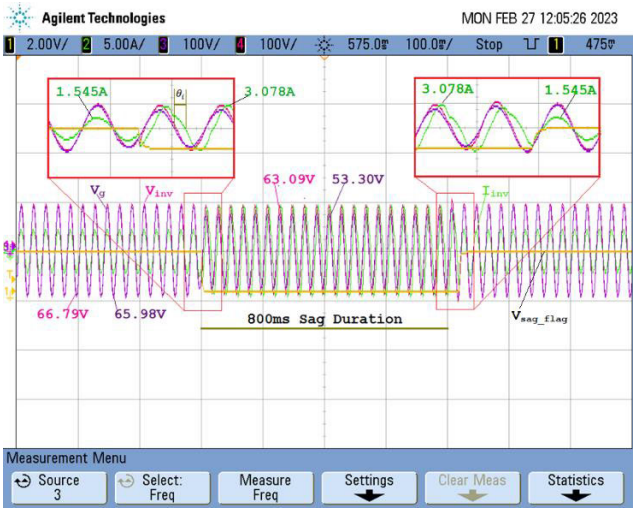

FIGURE 12. Experimental result illustrating auto-correction droop control with voltage restorer capability.

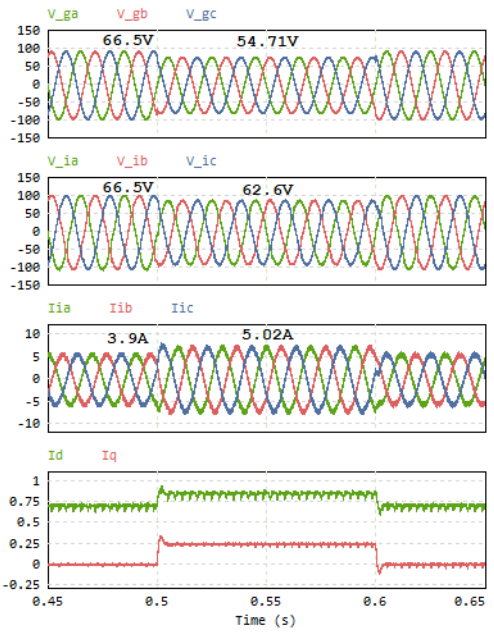

FIGURE 13. Simulation result illustrating the CAAPC mode under voltage sag ($k = 2.0$, and $k_d = 0.7$).

FIGURE 14. Experimental result illustrating the CAAPC mode under voltage sag ($k = 2.0$, and $k_d = 0.7$).

A. DGRE WITH VOLTAGE RESTORER CAPABILITY

When the grid voltage is normal, the proposed system operates primarily with auto-correction droop control. Active power is also injected into the main grid as a result of the inverter supporting the local load. In order to maintain the grid voltage, the CSRRF is used as a real-time measurement system to detect grid voltage sags. An accurate detection enables the system to determine how much reactive power to inject based on the capacity of the inverter to support the grid under voltage drop disturbance and may restore the grid voltage. As a result, the proposed droop control can maintain the PCC voltage.

Auto-correction droop control strategy restores the grid voltage after a sag by injecting proportional active and reactive power as illustrated in Figure 10. The grid voltage (v_g) drop from 66.5 V to 56.22 V at 0.5 s until 0.6 s has triggered the controller to restore V_{pcc} to the normal rated grid voltage by injecting the required active and reactive power to the primary grid. The grid voltage increases from 57.33 V to 65.94 V which indicates that it has been successfully restored. During the voltage restoration, the current increases from 3.93 A to 5.5 A. Moreover, when the grid voltage drops to 51.14 V, the controller attempts to restore the voltage to 59.61 V only, as depicted in Figure 11. Since 66.5 V is equivalent to 1.0 pu

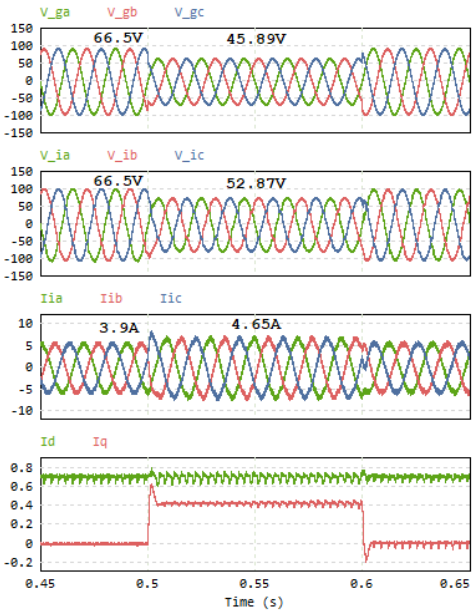

FIGURE 15. Simulation result illustrating constant active current (I_d) with CACC mode ($k = 2.0$, and $m = 0.7$).

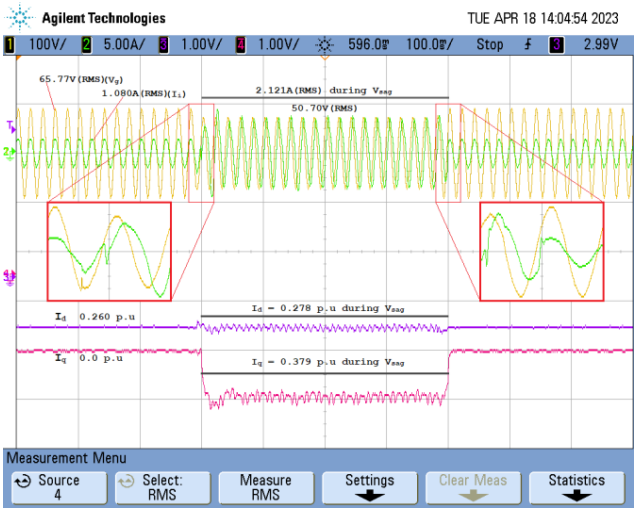

FIGURE 16. Experimental result illustrating constant active current (I_d) with CACC mode ($k = 2.0$, and $m = 0.7$).

FIGURE 17. Experimental result illustrating P and Q injection with CACC mode ($k = 2.0$, and $m = 0.7$).

then 65.94 V, 59.61 V, 57.33 V and 51.14 V are 0.992 pu, 0.896 pu, 0.862 pu and 0.769 pu, respectively. 0.78 pu is the critical value for the auto-correction droop control to restore V_{pcc} to the normal grid voltage. Since 0.769 pu is less than the critical value, the controller is not able to restore to the normal grid voltage. The increase in voltage is only up to 59.61 V or 0.896 pu, which is not enough to fully restore the voltage at 66.5 V or 1.0 pu.

Figure 12 illustrates the result of the first scenario to overcome the voltage sag. Under grid-connected operation, the grid voltage drops suddenly from 65.98 V (RMS) to 53.30 V (RMS) which are equivalent to 1.0 pu to 0.78 pu, respectively. As per the old grid code, the inverter should be disconnected from the primary grid. However, the new grid code allows the inverter to remain connected by injecting reactive power along with or without active power. Therefore, the proposed scheme supports an increase in inverter voltage to 63.09 V (RMS) with a 800 ms of sag duration which results in the inverter to increase current injection from 1.545 A to 3.078 A, where the current lags the voltage by 60^o. Despite the grid voltage sag, there no significant distortion in the injected current during the voltage drop, and the system able to regain stability quickly and precisely after the voltage drop ends.

B. DGRE WITH LVRT STRATEGY CAPABILITY

When voltage sag occurs in the second scenario, the inverter remains connected to the main grid in the LVRT mode of operation. Three LVRT modes are considered as explained below:

1) LVRT IN CAAPC MODE

The first mode of LVRT strategy is assigned to maximize power delivery. For this mode, the DGRE injects reactive current to handle voltage sag without reducing active current injection into the grid. As illustrated in Figure 13, this mode is simulated during the grid voltage drops from 66.5 V to 54.71 V. The DGRE responds by injecting active and reactive current that is reflected as increasing current from 3.9 A to 5.02 A. By applying CAAPC fast transient response can be achieved to handle the voltage sag.

Figure 14 illustrates the system's response to voltage sag, where the RMS grid voltage is programmed to drop from 65.77 V to 50.70 V over a time period of 800 ms. The constant average active power control is configured to handle grid voltage sag. Active power reference P_{ref} is fixed at 0.270 pu

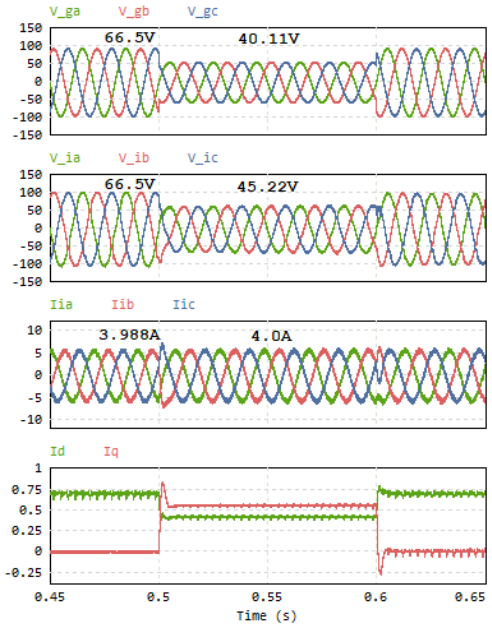

FIGURE 18. Simulation result illustrating CPCC strategy with constant $I_{g\ max}$ under voltage sag ($k = 2.0$, and $n = 0.5$).

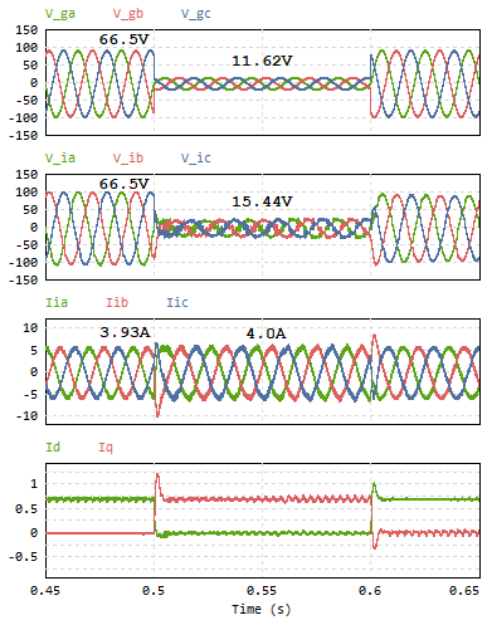

FIGURE 19. Simulation result illustrating CPCC mode under ultra weak grid voltage ($k = 2.0$, and $n = 0.5$).

TABLE 3. Comparison between LVRT modes during voltage sag (0.78 p.u.).

LVRT mode	Normal V_g			Transition	Voltage sag		
	I_i (A)	P (W)	Q(VAr)		I_i (A)	P(W)	Q (VAr)
CAAPC	1.51	270	0	current spike	3.044	270	263
CACC	1.08	213	0	Smooth	2.121	205	253
CPCC	1.531	302	0	Smooth	1.582	15	239

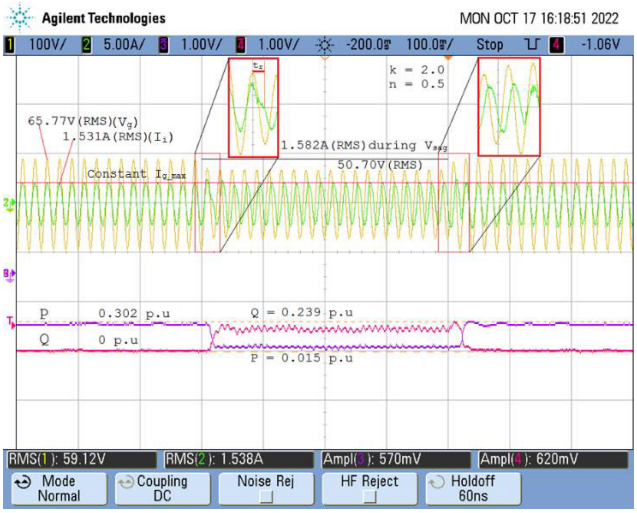

FIGURE 20. Experimental result illustrating CPCC mode with constant $I_{g\ max}$ under voltage sag ($k = 2.0$, and $n = 0.5$).

which equals 270 W, and reactive power reference Q_{ref} is fixed at 0.0 pu equalling 0 Var; these are displayed in CH3 and CH4 of Figure 14, respectively. Using a voltage sag detector, a sudden drop in voltage of the grid can be detected in real-time. With the RPI strategy, the inverter can remain connected to the grid in LVRT mode. The RPI can be identified with the grid current lagging the grid voltage. As shown in CH2 of Figure 11, inverter current increases during voltage sag, to maximize output energy of the inverter in handling voltage drop.

2) LVRT IN CACC MODE

The second LVRT mode namely CACC maintains active current during grid voltage drops. As depicted in Figure 15, grid voltage drops from 66.5 V to 45.89 V forces the DGRE to inject 0.4 pu of reactive current by maintaining 0.7 pu of active current. Hence, the CACC mode is able to maintain active current of 0.7 pu during the voltage sag with a smooth transient response achieved.

Figure 16 shows the result for the constant active current control of LVRT with parameters $k = 2$, and $m = 0.7$. The DGRE sets constant $I_d = 0.26$ pu and $I_q = 0.0$ pu for grid-connected operation. Since the grid voltage sag is detected, the DGRE reacts to inject reactive current and maintain its connection to the grid. The experiment has demonstrated that the DGRE generates 0.379 pu of reactive current during voltage sag. Meanwhile, the transition looks seamless, with fast and accurate response without any significant delay. It can be observed too that the current increases from 1.08 A to 2.121 A as a result of the voltage sag before it is restored once the voltage sag disappeared.

Figure 17 illustrates the experimental result of P and Q during normal and grid-connected operation. The DGRE initially generates 0.213 pu (213 W) and 0.0 pu (0 VAr) of P and Q, respectively. As a result of a voltage sag, the DGRE

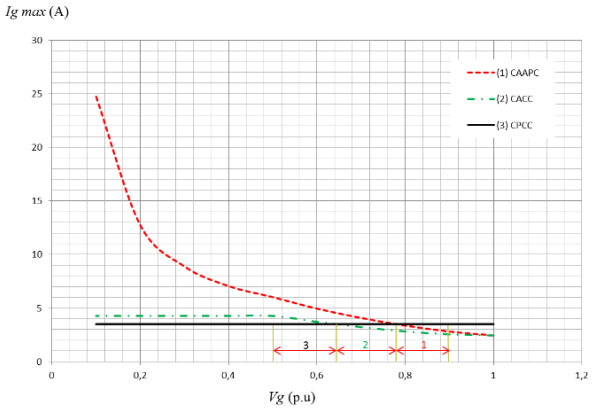

FIGURE 21. Required injected current for different LVRT modes.

generates 0.253 pu, which equals 253 VAr of Q to sustain the interconnection between the DGRE and the grid. However, P was reduced to 0.205 pu (205 W). It is also noted that the inverter current lags the inverter voltage by 60^o during the voltage sag.

3) LVRT IN CPCC MODE

The third LVRT mode is CPCC that assigned to limit the inverter current during a critical sag $\left(0 < V_g < 0.65\,pu\right)$. As illustrated in Figure 18, the grid voltage drop from 66.5 V to 40.11 V or 0.6 pu. In this situation, the DGRE with CPCC mode injects 0.55 pu of reactive current and reduces the active current from 0.7 pu to 4.0 pu. In order to ensure current of the DGRE remains constant (4.0 A).

In case of critical voltage sag, the DGRE with CPCC mode has been employed to avoid islanding condition. Figure 19 shows the result of simulation to validate the proposed strategy under ultra weak grid fault. The grid voltage drops from 66.5 V to 11.62 V in a duration of 0.1 s. Consequently, the DGRE reacts by injecting 0.7 pu of active current and reduces the active current to zero. Therefore, the DGRE maintains the peak current.

Figure 20 depicts the result of the constant peak current control, which offers inverter overcurrent protection. The experiment has been set up for $k = 2$, and $n = 0.5$, which results in an inverter voltage of 65.77 V (RMS) and an inverter current of 1.531 A (RMS) during the normal grid-connected operation. The inverter injects 0.302 pu (302 W) of P and 0 pu (0 VAr) of Q during this operation. Owing to the voltage drops in the line networks, the system cannot support restoring the voltage. As a result, the controller reacts to inject Q by maintaining the inverter peak current with P reduction. Under the sag condition, the inverter limits the injected current, increases Q, and reduces P to 1.582 A (RMS), 0.239 p.u (239 VAr), and 0.015 pu (15 W), respectively. The controller records an accurate and fast response to maintain the peak current and shift the phase angle by about $\frac{\pi}{3}$. The response time (t_r) to achieve the required phase angle is about half a cycle of the voltage period (0.01 s).

TABLE 4. Comparison of the LVRT modes.

LVRT mode	Advantage	Disadvantage
CAAPC	Maximum energy delivery	Overshoot current transition possibility, derating the inverter
CACC	Low current rating	Derating the inverter
CPCC	Overcurrent protection capability	Active power reduction

4) PERFORMANCE COMPARISON OF THE LVRT STRATEGY

As presented in Table 3, three different modes have been presented to validate the effectiveness of the LVRT strategy. Based on the experimental results, the three modes perform satisfactorily well in handling voltage sag disturbances by providing reactive power injection. CAAPP can support voltage sag operation by injecting 263 VAr of reactive power and maintaining 270 W of active power. This leads to a maximum power delivery to the primary grid. Nonetheless, the current spike that was observed, can be a concern. CACC reduces the current spike by limiting the active current. Under normal grid-connected operation, CACC generates lower current compared to other LVRT modes. As presented in Table 3, CACC generates 1.08 A of injected current, with 213 W of injected active power. Meanwhile, during voltage sag condition, CACC records a slight reduction in the active power (205 W) while injecting 253 VAr of reactive power, leading to an increase in the inverter current. As for the CPCC mode, the injected active power reduces dramatically from 302 W to 15 W during the transition from normal grid-connected operation to voltage sag operation. At the same time, a reactive power of 239 VAr has been injected, resulting in a slight increase in the inverter current from 1.531 A to 1.582 A.

Figure 21 shows the performance comparison between CAAPC, CACC, and CPCC based on the injected current. Here, the injected current is calculated using equations (37), (39) – (40), and (44) – (47). Similar parameter values utilized in the experiment are also used in the calculation i.e., $I_N = 3.5$A, $k = 2$, $k_d = 0.7$, $m = 0.7$, and $n = 0.5$. The nominal current injection I_N is limited to 3.5 A. Depending on the level of voltage drop and the DGRE capacity, each LVRT mode exhibits better performance in comparison to the others. It is observed that for CAAPC to be effectively operated, the effective operating range is $0.78 < v_g < 0.9$. In this voltage range, CAAPC and CACC generate current less than I_N, which is considered safe for the DGRE. However, since CAAPC injects more current (below I_N) than the CACC, CAAPC would then inject optimum power to the grid as compared to that of the CACC. As for CACC, it is effectively operated for $0.65 < v_g < 0.78$, since the injected current is below I_N while other LVRT modes would inject current more than I_N. For the operating range of $0.5 < v_g < 0.65$, only CPCC can achieve effective operation as the injected current equals I_N while other LVRT modes are not able to meet the I_N constraint.

The summary of the LVRT modes are shown in Table 4. The main advantage of CAAPC mode is the fact that it maximizes output power. However, this mode is derating the inverter, and overshoot current appears in the falling edge of the sag transition. Consequently, the inverter must use high current ratings for the switching components to avoid high stress and increasing temperature. As for the CACC strategy, despite derating the inverter, this mode offers a reduction in the stress and temperature of the switching components during LVRT operation. This mode shows a seamless transition and holds the active power before, during, and after voltage sag, thus preventing from achieving maximum energy delivery. On the other hand, the CPCC mode offers overcurrent protection capability despite its drawback in reducing active power.

C. PERFORMANCE COMPARISON BETWEEN THE PROPOSED STRATEGY AND THE OTHER TECHNIQUES

There are 10 out of 13 research teams who carried out experimental validation of their respective techniques as listed in Table 1. Among these, there are two techniques that employ Dynamics Voltage Restorer for voltage sag compensation [23], [33]. Seven methods present the LVRT strategy with varying test cases and conditions [3], [21], [24], [25], [26], [29], [31]. Additionally, the droop control strategy is also presented by [32] to handle grid voltage sag. Unlike all these techniques, the proposed method combines the LVRT algorithm with autocorrection droop control scheme to enhance its capability in handling voltage sag. The autocorrection droop control feature can restore the voltage drop by injecting active and reactive power if the apparent power is less than the maximum generated apparent power. However, if it exceeds the maximum generated apparent power, the LVRT strategy is employed to handle voltage sag. Three LVRT modes have been introduced and they operate in manner to optimize power injection based on the level of grid voltage drops.

Based on the experimental results, the DVR methods pesented by [23] and [33] have been used as a means of compensating for grid voltage drop through the injection of the required voltage, as depicted in Figures 22(a) and Figure 22(b). Both methods respond promptly in managing voltage sag and restoring the grid voltage. On the other hand, the proposed strategy illustrated in Figure 22(c) restores PCC voltage to the typical grid voltage by injecting reactive power. These methods share a common goal of rectifying the voltage during a voltage sag. However, the strategy in [23] and [33] cease injecting the required voltage during normal grid operations, a contrast to the proposed strategy, which can inject active power during normal grid operations and inject active and reactive power during grid voltage sag to restore the PCC voltage.

In addition, a current limiter droop control has been presented by [32]. The objective of this approach is to optimize power injection into the primary grid during grid faults, achieved through the injection of active and reactive power.

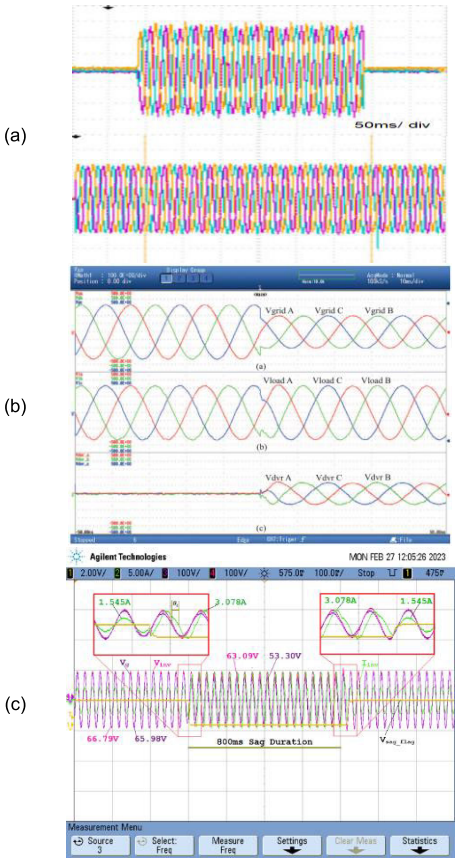

FIGURE 22. Comparison of experimental result on the voltage restorer performance. (a) [23], (b) [33], (c) [this paper].

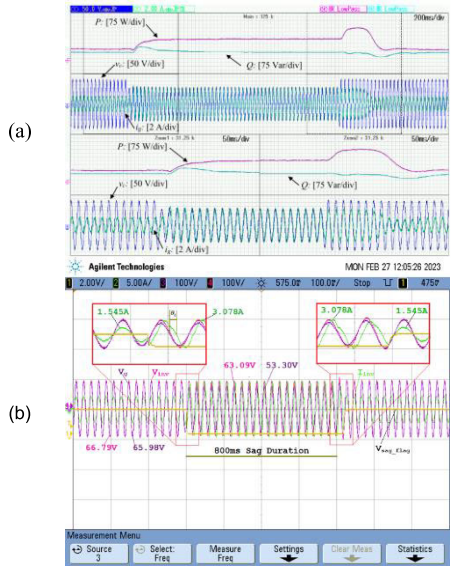

FIGURE 23. Experimental result for advanced droop control strategy (a) current limiting droop control [32], (b) autocorrection droop control [this paper].

It has been found that this strategy has a limitation in post-fault transient conditions, where the controller exhibits a slow response to achieve a steady state current after the sag

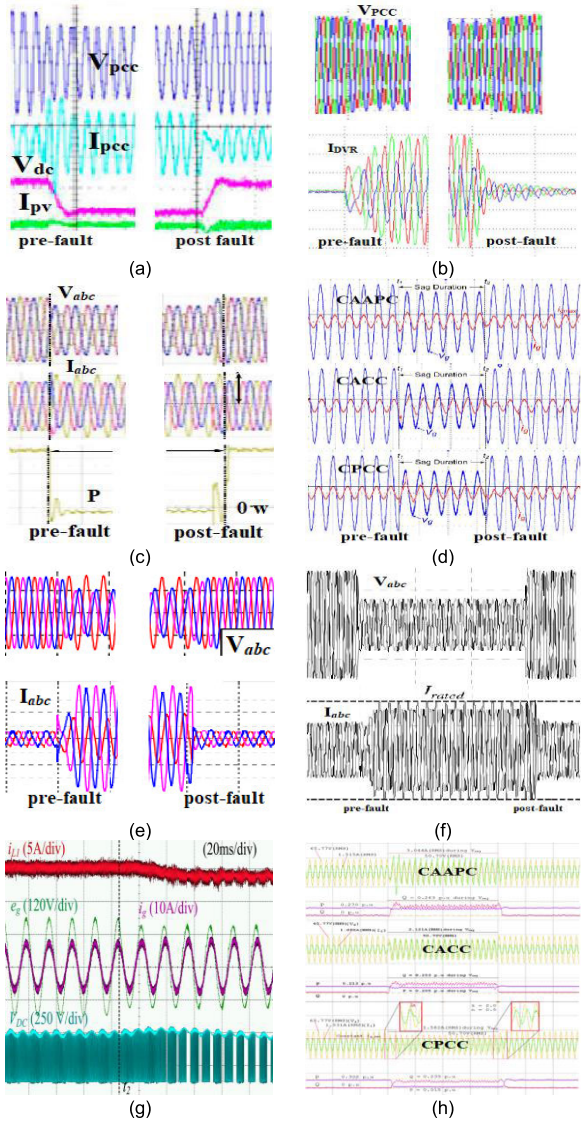

FIGURE 24. Performance comparison among several LVRT. (a) He et.al [3], (b) Zhao et.al [21], (c) Chen et.al [24], (d) Yang et.al [25], (e) Sosa et.al [26], (f) Lopez et.al [29], [g] Easley et.al [31], (h) [This Paper].

has disappeared. It can be observed in Figure 23(a) that more than eight cycles were required to reach a steady state after the fault vanished. This response time is relatively slow compared to the proposed strategy, which can attain a steady-state condition in less than one cycle after the fault has disappeared, as demonstrated in Figure 23(b).

The proposed strategy incorporates multiple LVRT modes including CAAPC, CACC, and CPCC with autocorrection droop control to manage grid voltage sag. The chosen mode is determined by the level of voltage drop. The proposed approach strives to inject optimal active power into the primary grid until it can no longer deliver active power. At this point, reactive power injection becomes necessary to resolve the voltage sag. Here, the proposed approach offers several advantages to ensure that the DG remains connected to the primary grid, primarily when autocorrection droop control and LVRT algorithms are utilized. To verify performance, the controller response can be evaluated during pre-fault and post-fault conditions, explicitly looking at overshoot current and delay response as indicators of the proposed approach effectiveness in handling faults.

Figure 24 exhibits eight distinct techniques for handling grid voltage drop, including the proposed strategy. The pre-fault and post-fault transient responses are analyzed and compared, while post-fault power recovery and voltage support capability are discussed and highlighted by [3]. Notably, Figure 24(a) depicts the overshoot current at the PCC (I_{pcc}) during the pre-fault condition, as opposed to the results provided by [21], which indicate a five-cycle delay to achieve a steady state during the post-fault situation. Fast response times during both pre-fault and post-fault conditions are achieved by [24] and [25] and the proposed strategy, as illustrated in Figure 24(c), (d), and (h), respectively. However, both techniques serve different objectives, with [24] minimizing power ripple during active and reactive power injection and [25] presenting maximum power injection while reducing overcurrent during voltage sag. Furthermore, the experimental results indicate a one-cycle delay of the pre-fault response, which was utilized by [26] to maximize power delivery during sag conditions. Figure 24(f) shows the experimental results of [29], wherein pre-fault and post-fault transient responses show a one-cycle delay while implementing the inverter capability to deliver power to the primary grid. In reference [31], a seamless transition with a slow transient response during voltage sag can be observed in Figure 24(g).

V. CONCLUSION

Either under normal or under voltage sag conditions, the system successfully maintains energy delivery to the primary grid. Adaptive power control is introduced by auto-correction droop control to regulate P and Q in accordance with network impedance. It is possible to support grid operation under normal or voltage sag conditions by proportionally generating P and Q based on the capacity of the inverters. By adopting an LVRT strategy and ensuring that the inverter remains connected during voltage sag, the proposed strategy prevents overcurrent injection beyond the inverter's capacity. A LVRT strategy can be implemented in three different ways, each with its own advantages and disadvantages. Based on the experimental results, the three modes provide a fast and accurate response when handling voltage sags. Despite the fact that there may be overshoot currents in the falling edge of the voltage sag, the CAAPC provides the full power delivery to sustain the primary grid. By restoring voltage at the PCC, the proposed droop control works well to maintain the grid voltage.

REFERENCES

[1] D. M. Vilathgamuwa, P. C. Loh, and Y. Li, "Protection of microgrids during utility voltage sags," *IEEE Trans. Ind. Electron.*, vol. 53, no. 5, pp. 1427–1436, Oct. 2006, doi: 10.1109/TIE.2006.882006.

[2] H. Dehghani Tafti, A. I. Maswood, G. Konstantinou, J. Pou, and P. Acuna, "Active/reactive power control of photovoltaic grid-tied inverters with peak current limitation and zero active power oscillation during unbalanced voltage sags," *IET Power Electron.*, vol. 11, no. 6, pp. 1066–1073, May 2018, doi: 10.1049/iet-pel.2017.0210.

[3] Y. He, M. Wang, Y. Jia, J. Zhao, and Z. Xu, "Low-voltage ride-through control for photovoltaic generation in the low-voltage distribution network," *IET Renew. Power Gener.*, vol. 14, no. 14, pp. 2727–2737, Oct. 2020, doi: 10.1049/iet-rpg.2019.1101.

[4] R. Ntare, N. H. Abbasy, and K. H. M. Youssef, "Low voltage ride through control capability of a large grid connected PV system combining DC chopper and current limiting techniques," *J. Power Energy Eng.*, vol. 7, no. 1, pp. 62–79, 2019, doi: 10.4236/jpee.2019.71004.

[5] H. R. Baghaee, M. Mirsalim, G. B. Gharehpetian, and H. A. Talebi, "A new current limiting strategy and fault model to improve fault ride-through capability of inverter interfaced DERs in autonomous microgrids," *Sustain. Energy Technol. Assessments*, vol. 24, pp. 71–81, Dec. 2017, doi: 10.1016/j.seta.2017.02.004.

[6] N. Bottrell and T. C. Green, "Comparison of current-limiting strategies during fault ride-through of inverters to prevent latch-up and wind-up," *IEEE Trans. Power Electron.*, vol. 29, no. 7, pp. 3786–3797, Jul. 2014, doi: 10.1109/TPEL.2013.2279162.

[7] B. Fan, T. Liu, F. Zhao, H. Wu, and X. Wang, "A review of current-limiting control of grid-forming inverters under symmetrical disturbances," *IEEE Open J. Power Electron.*, vol. 3, pp. 955–969, 2022, doi: 10.1109/OJPEL.2022.3227507.

[8] W. Deng, N. Dai, K.-W. Lao, and J. M. Guerrero, "A virtual-impedance droop control for accurate active power control and reactive power sharing using capacitive-coupling inverters," *IEEE Trans. Ind. Appl.*, vol. 56, no. 6, pp. 6722–6733, Nov. 2020, doi: 10.1109/TIA.2020.3012934.

[9] U. B. Tayab, M. A. B. Roslan, L. J. Hwai, and M. Kashif, "A review of droop control techniques for microgrid," *Renew. Sustain. Energy Rev.*, vol. 76, pp. 717–727, Sep. 2017, doi: 10.1016/j.rser.2017.03.028.

[10] Q.-C. Zhong, "Robust droop controller for accurate proportional load sharing among inverters operated in parallel," *IEEE Trans. Ind. Electron.*, vol. 60, no. 4, pp. 1281–1290, Apr. 2013, doi: 10.1109/TIE.2011.2146221.

[11] C. K. Sao and P. W. Lehn, "Autonomous load sharing of voltage source converters," *IEEE Trans. Power Del.*, vol. 20, no. 2, pp. 1009–1016, Apr. 2005, doi: 10.1109/tpwrd.2004.838638.

[12] Y. W. Li and C.-N. Kao, "An accurate power control strategy for power-electronics-interfaced distributed generation units operating in a low-voltage multibus microgrid," *IEEE Trans. Power Electron.*, vol. 24, no. 12, pp. 2977–2988, Dec. 2009.

[13] D. Wu, F. Tang, J. M. Guerrero, J. C. Vasquez, G. Chen, and L. Sun, "Autonomous active and reactive power distribution strategy in islanded microgrids," in *Proc. IEEE Appl. Power Electron. Conf. Exposit. (APEC)*, Mar. 2014, pp. 2126–2131, doi: 10.1109/APEC.2014.6803600.

[14] H. Mahmood, D. Michaelson, and J. Jiang, "Reactive power sharing in islanded microgrids using adaptive voltage droop control," *IEEE Trans. Smart Grid*, vol. 6, no. 6, pp. 3052–3060, Nov. 2015, doi: 10.1109/TSG.2015.2399232.

[15] D. K. Dheer, Y. Gupta, and S. Doolla, "A self-adjusting droop control strategy to improve reactive power sharing in islanded microgrid," *IEEE Trans. Sustain. Energy*, vol. 11, no. 3, pp. 1624–1635, Jul. 2020, doi: 10.1109/TSTE.2019.2933144.

[16] S. Chakraborty, S. Patel, G. Saraswat, A. Maqsood, and M. V. Salapaka, "Seamless transition of critical infrastructures using droop controlled grid-forming inverters," *IEEE Trans. Ind. Electron.*, vol. 71, no. 2, 2024, Art. no. 15351546, doi: 10.1109/TIE.2023.3253946.

[17] F. Ismail, J. Jamaludin, and N. A. Rahim, "Improved active and reactive power sharing on distributed generator using auto-correction droop control," *Electric Power Syst. Res.*, vol. 220, Jul. 2023, Art. no. 109358, doi: 10.1016/j.epsr.2023.109358.

[18] Q.-C. Zhong and Y. Zeng, "Universal droop control of inverters with different types of output impedance," *IEEE Access*, vol. 4, pp. 702–712, 2016, doi: 10.1109/ACCESS.2016.2526616.

[19] N. Pogaku, M. Prodanovic, and T. C. Green, "Modeling, analysis and testing of autonomous operation of an inverter-based microgrid," *IEEE Trans. Power Electron.*, vol. 22, no. 2, pp. 613–625, Mar. 2007, doi: 10.1109/tpel.2006.890003.

[20] S. Sreekumar, D. S. Kumar, and J. S. Savier, "A case study on self healing of smart grid with islanding and inverter volt–VAR function," *IEEE Trans. Ind. Appl.*, vol. 56, no. 5, pp. 5408–5416, Sep. 2020.

[21] *Grid Code: High and Extra High Voltage*, E. ON Netz GmbH, Bayreuth, Germany, 2006, pp. 1–50.

[22] C.-Y. Tang, Y.-T. Chen, and Y.-M. Chen, "PV power system with multi-mode operation and low-voltage ride-through capability," *IEEE Trans. Ind. Electron.*, vol. 62, no. 12, pp. 7524–7533, Dec. 2015.

[23] X. Zhao, L. Chang, R. Shao, and K. Spence, "Power system support functions provided by smart inverters—A review," *CPSS Trans. Power Electron. Appl.*, vol. 3, no. 1, pp. 25–35, Mar. 2018.

[24] X. Guo, Z. Lu, B. Wang, X. Sun, L. Wang, and J. M. Guerrero, "Dynamic phasors-based modeling and stability analysis of droop-controlled inverters for microgrid applications," *IEEE Trans. Smart Grid*, vol. 5, no. 6, pp. 2980–2987, Nov. 2014, doi: 10.1109/TSG.2014.2331280.

[25] W. Rui, S. Qiuye, Z. Pinjia, G. Yonghao, Q. Dehao, and W. Peng, "Reduced-order transfer function model of the droop-controlled inverter via Jordan continued-fraction expansion," *IEEE Trans. Energy Convers.*, vol. 35, no. 3, pp. 1585–1595, Sep. 2020, doi: 10.1109/TEC.2020.2980033.

[26] *IEEE Standard for Interconnecting Distributed Resources with Electric Power Systems*, IEEE Standard 1547, 2003.

[27] A. Micallef, M. Apap, C. Spiteri-Staines, and J. M. Guerrero, "Single-phase microgrid with seamless transition capabilities between modes of operation," *IEEE Trans. Smart Grid*, vol. 6, no. 6, pp. 2736–2745, Nov. 2015, doi: 10.1109/TSG.2015.2444912.

[28] X. Zhao, J. M. Guerrero, M. Savaghebi, J. C. Vasquez, X. Wu, and K. Sun, "Low-voltage ride-through operation of power converters in grid-interactive microgrids by using negative-sequence droop control," *IEEE Trans. Power Electron.*, vol. 32, no. 4, pp. 3128–3142, Apr. 2017, doi: 10.1109/TPEL.2016.2570204.

[29] Y. Kumsuwan and Y. Sillapawicharn, "A fast synchronously rotating reference frame-based voltage sag detection under practical grid voltages for voltage sag compensation systems," in *Proc. 6th IET Int. Conf. Power Electron., Mach. Drives (PEMD)*, Mar. 2012, pp. 1–5, doi: 10.1049/cp.2012.0348.

[30] P. Li, L. Xie, J. Han, S. Pang, and P. Li, "A new voltage compensation philosophy for dynamic voltage restorer to mitigate voltage sags using three-phase voltage ellipse parameters," *IEEE Trans. Power Electron.*, vol. 33, no. 2, pp. 1154–1166, Feb. 2018, doi: 10.1109/TPEL.2017.2676681.

[31] H.-C. Chen, C.-T. Lee, P.-T. Cheng, R. Teodorescu, and F. Blaabjerg, "A low-voltage ride-through technique for grid-connected converters with reduced power transistors stress," *IEEE Trans. Power Electron.*, vol. 31, no. 12, pp. 8562–8571, Dec. 2016.

[32] Y. Yang, H. Wang, and F. Blaabjerg, "Reactive power injection strategies for single-phase photovoltaic systems considering grid requirements," *IEEE Trans. Ind. Appl.*, vol. 50, no. 6, pp. 4065–4076, Nov. 2014.

[33] J. L. Sosa, M. Castilla, J. Miret, J. Matas, and Y. A. Al-Turki, "Control strategy to maximize the power capability of PV three-phase inverters during voltage sags," *IEEE Trans. Power Electron.*, vol. 31, no. 4, pp. 3314–3323, Apr. 2016.

[34] X. Liu, C. Li, M. Shahidehpour, Y. Gao, B. Zhou, Y. Zhang, J. Yi, and Y. Cao, "Fault current hierarchical limitation strategy for fault ride-through scheme of microgrid," *IEEE Trans. Smart Grid*, vol. 10, no. 6, pp. 6566–6579, Nov. 2019, doi: 10.1109/TSG.2019.2907545.

[35] L. Ji, J. Shi, Q. Hong, Y. Fu, X. Chang, Z. Cao, Y. Mi, Z. Li, and C. Booth, "A multi-objective control strategy for three phase grid-connected inverter during unbalanced voltage sag," *IEEE Trans. Power Del.*, vol. 36, no. 4, pp. 2490–2500, Aug. 2021, doi: 10.1109/TPWRD.2020.3025158.

[36] M. A. Garnica López, J. L. G. de Vicuña, J. Miret, M. Castilla, and R. Guzmán, "Control strategy for grid-connected three-phase inverters during voltage sags to meet grid codes and to maximize power delivery capability," *IEEE Trans. Power Electron.*, vol. 33, no. 11, pp. 9360–9374, Nov. 2018, doi: 10.1109/TPEL.2018.2792478.

[37] D. I. Brandao, F. E. G. Mendes, R. V. Ferreira, S. M. Silva, and I. A. Pires, "Active and reactive power injection strategies for three-phase four-wire inverters during symmetrical/asymmetrical voltage sags," *IEEE Trans. Ind. Appl.*, vol. 55, no. 3, pp. 2347–2355, May 2019, doi: 10.1109/TIA.2019.2893135.

[38] M. Easley, S. Jain, M. Shadmand, and H. Abu-Rub, "Autonomous model predictive controlled smart inverter with proactive grid fault ride-through capability," *IEEE Trans. Energy Convers.*, vol. 35, no. 4, pp. 1825–1836, Dec. 2020.

[39] A. G. Paspatis, G. C. Konstantopoulos, and J. M. Guerrero, "Enhanced current-limiting droop controller for grid-connected inverters to guarantee stability and maximize power injection under grid faults," *IEEE Trans. Control Syst. Technol.*, vol. 29, no. 2, pp. 841–849, Mar. 2021.

[40] A. Parreño Torres, P. Roncero-Sánchez, J. Vázquez, Fco. J. López-Alcolea, and E. J. Molina-Martínez, "A discrete-time control method for fast transient voltage-sag compensation in DVR," *IEEE Access*, vol. 7, pp. 170564–170577, 2019, doi: 10.1109/ACCESS.2019.2955177.

[41] B. Mirafzal and A. Adib, "On grid-interactive smart inverters: Features and advancements," *IEEE Access*, vol. 8, pp. 160526–160536, 2020, doi: 10.1109/ACCESS.2020.3020965.

[42] T. Stetz, F. Marten, and M. Braun, "Improved low voltage grid-integration of photovoltaic systems in Germany," *IEEE Trans. Sustain. Energy*, vol. 4, no. 2, pp. 534–542, Apr. 2013, doi: 10.1109/TSTE.2012.2198925.

[43] *IEEE Standard for Interconnection and Interoperability of Distributed Energy Resources with Associated Electric Power Systems Interfaces*, IEEE Standard 1547, 2018.

[44] J. Lamb and B. Mirafzal, "Grid-interactive cascaded H-bridge multilevel converter PQ plane operating region analysis," *IEEE Trans. Ind. Appl.*, vol. 53, no. 6, pp. 5744–5752, Nov. 2017, doi: 10.1109/TIA.2017.2726498.

[45] J. Lamb, B. Mirafzal, and F. Blaabjerg, "PWM common mode reference generation for maximizing the linear modulation region of CHB converters in islanded microgrids," *IEEE Trans. Ind. Electron.*, vol. 65, no. 7, pp. 5250–5259, Jul. 2018, doi: 10.1109/TIE.2017.2777401.

[46] J. M. Guerrero, N. Berbel, J. Matas, L. G. De Vicuña, and J. Miret, "Decentralized control for parallel operation of distributed generation inverters in microgrids using resistive output impedance," in *Proc. IECON Ind. Electron. Conf.*, Nov. 2006, vol. 54, no. 2, pp. 5149–5154, doi: 10.1109/IECON.2006.347859.

[47] Y. Bae, T.-K. Vu, and R.-Y. Kim, "Implemental control strategy for grid stabilization of grid-connected PV system based on German grid code in symmetrical low-to-medium voltage network," *IEEE Trans. Energy Convers.*, vol. 28, no. 3, pp. 619–631, Sep. 2013, doi: 10.1109/TEC.2013.2263885.

FAUZAN ISMAIL received the B.E. degree from the University of Andalas, Padang, Indonesia, in 2004, and the M.Eng.Sc. degree in power electronics from the University of Malaya (UM), Kuala Lumpur, Malaysia, in 2011, where he is currently pursuing the Ph.D. degree in power electronics.

In 2016, he joined the Department of Electrical Engineering, Padang Institute of Technology, as a Lecturer. Since 2019, he has been a Research Assistant with the UM Power Energy Dedicated Advanced Centre, University of Malaya. His research interests include power electronics and renewable energy.

JAFFERI JAMALUDIN (Member, IEEE) received the B.Eng. degree from Universiti Tenaga Nasional, Putrajaya, Malaysia, and the M.Eng.Sc. and Ph.D. degrees from the University of Malaya (UM), Kuala Lumpur, Malaysia.

From 2018 to 2019, he was a Visiting Lecturer with the Department of System Design Engineering, Keio University, Japan. He is currently a Senior Lecturer with the UM Power Energy Dedicated Advanced Centre (UMPEDAC). His research interests include power electronics, controller design, and energy management.

Dr. Jamaludin is a member of the Institution of Engineering and Technology, U.K. He is also a Professional Technologist, Malaysia, and a Chartered Engineer, U.K.

NASRUDIN ABD RAHIM (Senior Member, IEEE) received the B.Sc. (Hons.) and M.Sc. degrees from the University of Strathclyde, Glasgow, U.K., and the Ph.D. degree from Heriot–Watt University, Edinburgh, U.K., in 1995.

He is currently a Professor with the University of Malaya (UM), Kuala Lumpur, Malaysia, where he is also the Director of the UM Power Energy Dedicated Advanced Centre. His research interests include power electronics, solar PV, real-time control systems, and electrical drives.

Dr. Rahim is a fellow of the Institution of Engineering and Technology, U.K., and the Academy of Sciences Malaysia. He is also a Professional Engineer, Malaysia, and a Chartered Engineer, U.K.